Published online 11 May 2019

Nucleic Acids Research, 2019, Vol. 47, No. 12 ***6045–6058***
doi: 10.1093/nar/gkz360

Conjugation of hydrophobic moieties enhances potency of antisense oligonucleotides in the muscle of rodents and non-human primates

Michael E. Østergaard, Michaela Jackson, Audrey Low, Alfred E. Chappell, Richard G. Lee, Rachel Q. Peralta, Jinghua Yu, Garth A. Kinberger, Amy Dan, Rick Carty, Michael Tanowitz, Patrick Anderson, Tae-Won Kim, Linda Fradkin, Adam E. Mullick, Sue Murray, Frank Rigo, Thazha P. Prakash, C. Frank Bennett, Eric. E. Swayze, Hans J. Gaus and Punit P. Seth*

Ionis Pharmaceuticals, 2855 Gazelle Court, Carlsbad, CA 92010, USA

Received March 22, 2019; Revised April 18, 2019; Editorial Decision April 25, 2019; Accepted April 26, 2019

ABSTRACT

We determined the effect of attaching palmitate, tocopherol or cholesterol to PS ASOs and their effects on plasma protein binding and on enhancing ASO potency in the muscle of rodents and monkeys. We found that cholesterol ASO conjugates showed 5-fold potency enhancement in the muscle of rodents relative to unconjugated ASOs. However, they were toxic in mice and as a result were not evaluated in the monkey. In contrast, palmitate and tocopherol-conjugated ASOs showed enhanced potency in the skeletal muscle of rodents and modest enhancements in potency in the monkey. Analysis of the plasma-protein binding profiles of the ASO-conjugates by size-exclusion chromatography revealed distinct and species-specific differences in their association with plasma proteins which likely rationalizes their behavior in animals. Overall, our data suggest that modulating binding to plasma proteins can influence ASO activity and distribution to extra-hepatic tissues in a species-dependent manner and sets the stage to identify other strategies to enhance ASO potency in muscle tissues.

INTRODUCTION

Antisense oligonucleotides (ASOs) that interact with their target RNA in cells by Watson–Crick base-pairing have made significant advances in the clinic (1). Most ASOs in clinical development are modified using the phosphorothioate (PS) backbone modification which improves metabolic stability by enhancing resistance to nuclease-mediated degradation (2). The PS backbone also promotes association with plasma and cell-surface proteins which facilitates tissue distribution and cellular entry (3). While unconjugated PS-ASOs have shown excellent activity in clinical trials, ASGR-mediated ASO delivery to hepatocytes further enhanced potency by 30-fold in the clinic (4,5). Similarly, targeted delivery of PS-ASOs to pancreatic beta cells via the GLP1-receptor showed >40-fold increases in potency in preclinical rodent models (6). Despite these advancements, targeted delivery of ASOs to additional cell types and tissues remains a key hurdle to fully realize their potential in the clinic.

The skeletal muscle and heart represent tissues that offer numerous opportunities for developing ASO therapeutics. Muscle diseases such as Duchenne muscular dystrophy (DMD) and myotonic dystrophies (DM1) result from alterations in RNA-splicing or from accumulation of toxic RNA species, respectively (7,8). These diseases are uniquely amenable for treatment using ASO technology, which directly targets the disease-causing RNA (9). Drisapersen, a uniform 2′-OMe PS-ASO that causes exclusion of exon 51 in dystrophin mRNA, was investigated extensively as a potential treatment for DMD (10). Similarly, additional ASO therapeutics to treat muscle disorders are currently in pre-clinical and clinical development (11,12). While PS ASOs can be effectively delivered to muscle tissues in rodent models of muscle diseases, doses required to elicit antisense pharmacology are typically higher than what are needed to show antisense effects in the liver (13). This can result in dose-limiting toxicities in the clinic as seen for Drisapersen (14). Thus, strategies which enhance ASO delivery to muscle tissues could greatly enhance efficacy and help deliver diseases-modifying treatments to patients.

Tissues such as the skeletal muscle and heart are accessible to PS ASOs from the systemic circulation after subcutaneous or intravenous injection (15). However, unlike the liver which has a sinusoidal capillary architecture, or the kidney which has a fenestrated endothelium, the continuous

*To whom correspondence should be addressed. Tel: +1 760 603 2587; Email: pseth@ionisph.com

© The Author(s) 2019. Published by Oxford University Press on behalf of Nucleic Acids Research.
This is an Open Access article distributed under the terms of the Creative Commons Attribution Non-Commercial License (http://creativecommons.org/licenses/by-nc/4.0/), which permits non-commercial re-use, distribution, and reproduction in any medium, provided the original work is properly cited. For commercial re-use, please contact journals.permissions@oup.com

endothelium of the muscle represents a significant barrier for efficient delivery of macromolecular therapeutics (16). PS ASOs are highly polar anionic macromolecules which cannot transit across the capillary endothelium by the paracellular route and require delivery into the interstitium of the muscle by transcytosis prior to entry into muscle cells.

Plasma proteins such as albumin and lipoproteins are known to be efficiently transported across the endothelium (17). Indeed, almost 60% of total albumin resides outside the vasculature in the interstitial spaces of muscle, skin and adipose tissues, and other fluids (18). It has been estimated that albumin makes ∼28 trips in and out of the lymphatic system during its lifetime as it shuttles between the extravascular space and the blood compartment (19). Thus, enhancing association of PS ASOs with plasma proteins such as albumin and lipoproteins represents one strategy to facilitate ASO delivery across the endothelium and enhance ASO potency in muscle tissues.

Conjugation of hydrophobic moieties to single and double stranded nucleic acids to modulate pharmacokinetic and cellular uptake properties has received significant attention over the past two decades (20,21). Recent work has shown that cholesterol and other fatty acids can modulate tissue distribution of siRNA to extra-hepatic tissues (22–26). Similarly, tocopherol ASO duplexes showed enhanced activity in the liver that was attributed to changes in plasma protein binding (27). We therefore investigated if conjugating hydrophobic moieties to single stranded PS ASOs can enhance ASO potency in muscle tissues by modulating interactions with plasma proteins.

In this report, we determined the effect of attaching palmitate, tocopherol or cholesterol to PS ASOs and their effects on plasma protein binding and on enhancing ASO potency in the muscle of rodents and monkeys. We found that cholesterol ASO conjugates showed 5-fold potency enhancement in the muscle of rodents relative to unconjugated ASOs. However, they were toxic in mice and as a result were not evaluated in the monkey. In contrast, palmitate and tocopherol-conjugated ASOs showed enhanced potency in the skeletal muscle of rodents and modest enhancements in potency in the monkey. Analysis of the plasma-protein binding profiles of the ASO-conjugates by size-exclusion chromatography revealed distinct and species-specific differences in their association with plasma proteins which likely rationalizes their behavior in animals. Overall, our data suggest that modulating binding to plasma proteins can influence ASO activity and distribution to extra-hepatic tissues in a species-dependent manner and sets the stage to identify other strategies to enhance ASO potency in muscle tissues.

MATERIALS AND METHODS

Synthesis of ASO conjugates

Oligonucleotides were synthesized using an AKTA Oligopilot scale using Nittophase unylinker support (317 μmol/g). Fully protected nucleoside phosphoramidites were purchased from commercial vendors and incorporated using standard solid-phase oligonucleotide synthesis, i.e. 15% dichloroacetic acid in toluene for deblocking, 1 M 4,5-dicyanoimidazole 0.1 M *N*-methylimidazole in acetonitrile as activator for amidite couplings, 20% acetic anhydride in THF and 10% 1-methylimidazole in THF/pyridine for capping, 10% tBuOOH in acetonitrile for oxidation and 0.1 M xanthane hydride in pyridine:acetonitrile 1:1 (v:v) for thiolation. Amidites were dissolved to 0.1 M in acetonitrile:toluene 1:1 (v:v) and incorporated using 6 min recycling time for DNA amidites and 10 min for all other amidites. At the end of the solid phase synthesis cyanoethyl protecting groups were removed by a 30 min. treatment with 20% diethylamine in toluene. Remaining protecting groups were removed in conc. aq. ammonia at 55°C for 8 h. Oligonucleotides were purified on a reverse phase column (Oligo S80 C18 Polymer). Failure sequences were eluted by flowing 40% MeOH, 1.25 M NaBr and 25 mM NaOH over the column for 3 min at 50 ml/min and desired compound eluted in 80% MeOH in water. Purity and mass of oligonucleotides was determined using ion-pair LCMS. ASOs with a 3′-Alexa Fluor 647 conjugate was synthesized as above, except using a C7-amino functionalized support (Glen Research, USA). After ASO purification, the free amine was used for conjugation to NHS activated AlexaFluor 647. Analytical data for the synthesized oligonucleotides is provided in Supplementary Figure S1.

Plasma protein binding assay and size exclusion

Evaluation of binding properties of lipid ASOs to plasma proteins utilizing fluorescence polarization and size exclusion chromatography were performed as described before with slight modifications. 5′-lipid-conjugated MALAT-1 ASOs with ALEXA647 at the 3′-end were utilized as tracer molecules and synthesized at Ionis Pharmaceuticals. Measurements were performed in 1× phosphate buffered saline (PBS) and assays were set up in 96-well Costar plates (black flat-bottomed non-binding) purchased from Corning, NY, USA. Binding was evaluated by adding ALEXA647-labeled ASOs to yield 2 nM concentration to each well containing 100 μl of protein from sub nM to low mM concentration. Readings were taken using the Tecan (Baldwin Park, CA, USA) InfiniteM1000 Pro instrument (λ_{ex} = 635 nm, λ_{em} = 675 nm). Using polarized excitation and emission filters, the instrument measures fluorescence perpendicular to the excitation plane (the 'P-channel') and fluorescence that is parallel to the excitation plane (the 'S-channel'). Millipolarization units (mP) were calculated as follows: $mP = [(S - P * G)/ (S + P \times G)] \times 1000$. The 'G-factor' is measured by the instrument as a correction for any bias toward the P channel. Polarization values of each ALEXA647-labeled ASO in 1× PBS at 2 nM concentration were subtracted from each measurement. K_d values were calculated with GraphPad Prism 5 software (GraphPad Software, La Jolla, CA, USA) using non-linear regression for curve fit assuming one binding site.

Size exclusion chromatography was performed utilizing a Zenix C 300 column (Sepax, Newark, DE, USA) in PBS with UV detection at 280 nm to monitor protein elution and fluorescence detection (λ_{ex} = 647 nm, λ_{em} = 675 nm) to monitor bound and unbound ASO. Plasma from human, mouse, rat or monkey (BioIVT, Westbury, NY, USA) and ALEXA647-labeled lipid-conjugated MALAT-1 ASOs at 5 μM concentration was used to record binding profiles.

Extraction and quantitation of palmitate-conjugated ASO concentrations in tissues by LCMS

Tissues were minced and 50–200 mg samples were homogenized in 500 μl homogenization buffer (0.5% NP40 substitute (Sigma-Aldrich, St. Louis, MO, USA) in Tris-buffered saline, pH8) with Lysing Matrix D beads (MPBio Santa Ana, CA, USA) on a ball mill homogenizer (Retsch Haan, Germany) at 30 Hz for 45 s. Standard curves of each ASO were established in 500 μl aliquots of control tissue homogenate (50–200-mg tissue/ml homogenization buffer). A 27-mer, fully PS, MOE/DNA oligonucleotide was added as an internal standard (IS) to all standard curves and study samples. Samples and standards were extracted with phenol/chloroform followed by solid-phase extraction (SPE) of the resulting aqueous extract using phenyl-functionalized silica sorbent (Biotage, Uppsala, Sweden). Eluate from SPE was dried down using a warm forced-air (nitrogen) evaporator and reconstituted in 100–200 μl 100uM EDTA. Samples were analyzed by LC–MS. Briefly, separation was accomplished using an 1100 HPLCMS system (Agilent Technologies, Wilmington, DE, USA) consisting of a quaternary pump, UV detector, a column oven, an autosampler and a single quadrupole mass spectrometer. Samples were injected on an X-bridge OST C18 column (2.1 × 50 mm, 2.5-μm particles; Waters, Milford, MA, USA) equipped with a SecurityGuard C18 guard column (Phenomenex, Torrance, CA, USA). The columns were maintained at 55°C. Tributylammonium acetate buffer (5 mM) and acetonitrile were used as the mobile phase at a flow rate of 0.3 ml/min. Acetonitrile was increased from 20% to 70% over 11 min. Mass measurements were made online using a single quadrupole mass spectrometer scanning 1000–2100 m/z in the negative ionization mode. Molecular masses were determined using ChemStation analysis package (Agilent, Santa Clara, CA, USA). Manual evaluation was performed by comparing a table of calculated m/z values corresponding to potential metabolites with the peaks present in a given spectrum. Peak areas from extracted ion chromatograms were determined for ASOs and IS and a trendline established using the calibration standards, plotting concentration of ASO against the ratio of the peak areas ASO/IS. Concentration of ASOs in study samples were determined using established trendlines and reported as μg ASO/g tissue.

Quantitation of tocopherol and cholesterol-conjugated ASO concentrations in tissues by anion exchange chromatography

Tissue concentrations of ASO were determined using anion exchange chromatography (AEX) coupled with a fluorescently labeled complementary detector oligonucleotide. For liver, kidney, heart and quadricep samples, 30–100 mg tissue was homogenized in 1 ml G2 buffer (Qiagen Hilden, Germany) with 10 U/ml proteinase K (Sigma-Aldrich, St Louis, MO, USA) in FastPrep lysing tubes (MPBio Santa Ana, CA, USA) using pyramidal granite lysing matrix on a ball mill homogenizer (Retsch Haan Germany) at 30 Hz for 45 s. Serum samples were diluted 1:2 in G2 buffer with 10 U/ml proteinase K. Standards were prepared for each ASO at 1 μM in control tissue homogenates or serum. Samples and standards were incubated at 42°C overnight to facilitate proteinase K proteolysis. Digested samples were diluted 1–1000-fold in control tissue digest. Serial dilutions of digested standards were prepared from 500 to 0.97 nM in control tissue digest. All samples and standards were then diluted further 1:2 with 2 μM PNA detector probe (a 14-mer peptide nucleic acid labeled at the 5′ terminus with ALEXA488 complementary to the center 14 bases of the ASOs) in AEX buffer A (25 mM Tris, pH 9; 2 M urea; 20% acetonitrile), heated to 80°C for 5 min, and incubated at least 1 h at room temperature to allow the PNA and ASO to hybridize. Samples were separated by AEX on a DNAPac PA200 4 × 25 mm column (Thermo Fisher Waltham, MA, USA) using a gradient of 0–0.5 M $NaClO_4$ over 10 min at 1 ml/min. ASO–PNA duplex was measured using a fluorescent detector (Ex488/Em520) and quantified using calibration curves established with standards prepared in respective tissue matrices. These AEX conditions were optimized to differentiate excess (unhybridized) PNA detector oligo, ASO–PNA duplex, and lipid-conjugated ASO–PNA duplex by retention time.

Evaluation of ASOs targeting MALAT1 in differentiated 3T3-L1 adipocytes

Undifferentiated 3T3-L1 cells were plated at 4000 cells per well in 96-well culture plates (Corning) in DMEM medium supplemented with 10% fetal bovine serum (Thermo Fisher). Cells were allowed to incubate at 37°C and 10% CO_2 until 100% confluence was reached. To differentiate the cells from preadipocytes into adipocytes, the media was aspirated and 100 μL per well of DMEM medium containing 10% fetal bovine serum, 0.83 μM insulin, 0.25 μM dexamethasone, and 0.25 isobutylmethylxanthine (Sigma Aldrich) was added to the cells and allowed to incubate for 48 h at 37°C and 10% CO_2. Media was then aspirated from the cells and 100 μl per well of DMEM medium containing 10% fetal bovine serum and 0.83 M insulin was added to the cells and allowed to incubate for 48 h at 37°C and 10% CO_2. Media was then aspirated and 100 μl per well of DMEM medium containing 10% fetal bovine serum was added to the cells and allowed to incubate for 48 h at 37°C and 10% CO_2 to fully differentiate the cells.

Upon completing the full differentiation protocol, 10 μl of 10× antisense oligonucleotide was added to each well. Cells were allowed to incubate for 48 hours post oligonucleotide addition at 37°C and 10% CO_2. Cells were then washed in 100 μl PBS (Corning) and lysed in 40 μl Ultra-Pure Guanidine Isothiocynate Solution (Thermo Fisher). RNA was extracted and purified using a glass fiber filter plate (pall #5072) and chiotropic salts. RNA expression levels were quantitated with quantitative reverse transcription PCR on the QuantStudio7 PCR instrument (Applied Biosystems). Briefly 10 μl RT-qPCR reactions containing 4 μl of RNA were run with Agpath-ID reagents (Applied Biosystems) and gene specific TaqMan primer probe set (Integrated DNA Technologies) following the manufacturer's instructions. Total RNA levels, measured with Quant-iT Ribogreen Reagent (Thermo Fisher), were used to normalize the RT-qPCR data. Primer Probe Set Sequences, Forward Sequence 5′-TGGGTTAGAGAAGGCGTGTACTG, Re-

verse Sequence 5′-TCAGCGGCAACTGGGAAA, Probe 5′-CGTTGGCACGACACCTTCAGGGACT.

Protocol for animal experiments

Animal experiments were conducted in accordance with the American Association for the Accreditation of Laboratory Animal Care guidelines and were approved by the Animal Welfare Committee (Cold Spring Harbor Laboratory's Institutional Animal Care and Use Committee guidelines). The animals were housed in micro-isolator cages on a constant 12-h light–dark cycle with controlled temperature and humidity and were given access to food and water *ad libitum*. Animals were randomly grouped, and all animals were included in data analysis except those found dead.

Evaluation of ASOs targeting MALAT-1 RNA in mice

6-week-old male C57BL/6 mice (Jackson Laboratories, Bar Harbor, ME, USA) were intravenously administered ASO formulated in saline at 3, 7 and 20 mg/kg on day 0 and day 8. Three days following the final injection, mice were euthanized. Blood was collected by cardiac puncture exsanguination with K_2-EDTA (Becton Dickinson Franklin Lakes, NJ, USA) and plasma separated by centrifugation at 10 000 rcf for 4 min at 4°C. Plasma transaminases and other markers for tolerability assessments were measured using a Beckman Coulter AU480 analyzer. Tissues were collected, weighed, flash frozen in liquid nitrogen and stored at –80°C.

Evaluation of ASOs targeting DMPK mRNA in mice

Six-week old male Balb-c mice ($n = 4$/group, Charles River Laboratories, Wilmington, MA, USA) were injected subcutaneously once weekly for 4 weeks with saline solutions of A-dmpk at 10, 20 or 40 mg/kg; or Palm-dmpk1, Palm-dmpk2 or Palm-dmpk3 at 5, 10 or 20 mg/kg. Two days following the final injection mice were euthanized and blood and tissues were collected as described for the MALAT-1 ASO above.

Evaluation of ASOs targeting DMPK mRNA in rats

Six-week old male Sprague Dawley rats ($n = 4$/group, Charles River Laboratories, Wilmington, MA, USA) were injected subcutaneously once weekly for 4 weeks with saline solutions of A-dmpk at 10, 20 or 40 mg/kg; or Palm-dmpk1, Palm-dmpk2 or Palm-dmpk3 at 5, 10 or 20 mg/kg. Two days following the final injection mice were euthanized and blood and tissues were collected as described for the MALAT-1 ASO above.

Evaluation of ASOs targeting DMPK mRNA by subcutaneous and intravenous injections in mice

Six-week old male Balb-c mice ($n = 4$/group, Charles River Laboratories, Wilmington, MA, USA) were injected subcutaneously once weekly for 4 weeks with saline solutions of A-dmpk, Palm-dmpk2, Toc-dmpk or Chol-dmpk at 10 mg/kg by subcutaneous or intravenous injections. Two days following the final injection mice were euthanized and blood and tissues were collected as described for the MALAT-1 ASO above.

Evaluation of Toc-dmpk and Chol-dmpk in mice using multiple doses

6-week old male Balb-c mice (n = 4/group, Charles River Laboratories, Wilmington, MA) were injected subcutaneously once weekly for four weeks with saline solutions of A-dmpk, Toc-dmpk or Chol-dmpk at 5, 10 or 20 mg/kg by intravenous injections. Three days following the final injection mice were euthanized and blood and tissues were collected as described for the MALAT ASO above.

Evaluation of Palm-dmpk2 and Toc-dmpk in monkeys

Male cynomolgus monkeys were obtained from Orient Bio Inc., Republic of Korea. All animal procedures were conducted utilizing protocols and methods approved by the Institutional Animal Care and Use Committee (IACUC) and were in compliance with Animal Welfare Act and Guide for the Care and Use of Laboratory Animals (by ILAR publication). For Palm-dmpk2, monkeys ($n = 4$/group) were injected subcutaneously every three days during the first week of the study (on Days 1, 3, 5 and 7) and then once weekly thereafter (on Days 14, 21, 28, 35, 42 and 49) with 10, 20 and 40 mg/kg of A-dmpk or Palm-dmpk2. Blood (0.5 ml) was collected from each animal on Days –7, 30 and 51 with K2-EDTA for hematology assessments. Animals were euthanized 48 h after the last dose on day 51 by exsanguinations following sedation using intravenous sodium thiopental. Organs were weighed and samples for mRNA and ASO accumulation were flash frozen in liquid nitrogen at necropsy and then stored frozen (approximately –80°C) until final analysis. For Toc-dmpk, protocols were identical except for the mode of delivery. ASOs were administered by intravenous infusion over 1 h with a dose volume of 10 ml/kg.

mRNA isolation from mouse tissues

Briefly, 50–100 mg of frozen tissue was homogenized with an Omni Tissue Homogenizer (Omni International) in guanidinium thiocyanate with 8% beta mercaptoethanol, and total RNA was isolated using the PureLink Pro 96 Total RNA Purification Kit (LifeTechnologies, Carlsbad, CA, USA) or the Qiagen RNeasy 96-well columns (Qiagen, Hilden, Germany). RNA was extracted following manufacturer's instructions with an on-column DNase digestion using 40 U of DNase per sample. RNA was extracted in 70–200 μl water and quantitated by total RNA measured by RiboGreen, RNA Quantitation Reagent (Molecular Probes). RNA was diluted in water and a standard curve was prepared using RNA extracted from saline treated animals.

mRNA isolation from monkey tissues

50 mg of tissue was dissected while on dry ice and then homogenized in 2 ml of guanidine isothiocyanate with 8% beta-mercaptoethanol. 250 μl of the lysate was added to 750 μl of Trizol LS, shaken 20× by hand and then incubated at room temperature for 5 min. 200 μl of chloroform was added to the sample and shaken 20× by hand and then incubated at room temperature for 2 min. Samples were spun at 10 000 rpm for 10 min at 4°C. Aqueous

phase was removed and added to an equal volume of isopropanol. Sample were vortexed and then added to Qiagen (Qiagen, Hilden, Germany) RNeasy 96-well columns. RNA was extracted following manufacturer's instructions with an on-column DNase digestion using 100 U of DNase. RNA was extracted in water and quantitated by spectrophotometer at A260. RNA was diluted to 2 ng/μl for RT-qPCR. A standard curve was prepared using RNA extracted from saline treated animals.

Protocol for quantitative reverse transcriptase polymerase chain reaction (qRT-PCR)

Reduction of target mRNA expression was determined by real time RT-PCR using StepOne RT-PCR machines (Applied Biosystems, Foster City, CA, USA). Briefly, RNA was extracted from about 50 to 100 mg tissue from each mouse as described above and mRNA was measured by qRT-PCR using Express One-Step SuperMix qRT-PCR Kit (Life Technologies, Carlsbad, CA, USA). Primers and probes for the PCR reactions were obtained from Integrated DNA technologies (IDT). The assay is based on a target-specific probe labeled with a fluorescent reporter and quencher dyes at opposite ends. The probe is hydrolyzed through the 5′-exonuclease activity of Taq DNA polymerase, leading to an increasing fluorescence emission of the reporter dye that can be detected during the reaction. Target RNA levels were normalized to cyclophilin mRNA expression or normalized to the levels of total RNA measured by RiboGreen, RNA Quantitation Reagent (Molecular Probes).

The sequences for the primers and probe used for mouse Malat-1 are 5′-TGGGTTAGAGAAGGCGTGTACTG-3′ for the forward primer, 5′-TCAGCGGCAACTGGGAAA-3′ for the reverse primer, and 5′-CGTTGGCACGACAC CTTCAGGGACT-3′ for the probe. Target RNA levels were normalized to cyclophilin mRNA expression. The sequences for the primers and probe used for mouse cyclophilin A are 5′-TCGCCGCTTGCTGCA-3′ for the forward primer, 5′-ATCGGCCGTGATGTCGA-3′ and 5′-CC ATGGTCAACCCCACCGTGTTCX -3′ for the probe.

The sequences for the primers and probe used for mouse DMPK are 5′-GACATATGCCAAGATTGTGC ACTAC-3′ for the forward primer, 5′-CACGAATGAGGT CCTGAGCTT-3′ for the reverse primer, and 5′-AACA CTTGTCGCTGCCGCTGGC-3′ for the probe. The sequences for the primers and probe used for rat DMPK are 5′- AGTTGCCTGTGTCAGACTTG-3′ for the forward primer, 5′-CCATGGTCTCTGTCTCAGC-3′ for the reverse primer, and 5′-TCTTCAGCCGCTTGATCCGG TG-3′ for the probe. Target RNA levels were normalized to the either the levels of total RNA measured by RiboGreen, RNA Quantitation Reagent (Molecular Probes) or to the levels of Gapdh. The sequences for the primers and probe used for mouse Gapdh are 5′-GGCAAATTCAACGGCACAGT-3′ for the forward primer, 5′-GGGTCTCGCTCCTGGAAGAT-3′ for the reverse primer, and 5′- AAGGCCGAGAATGGGAAGCT TGTCATC-3′ for the probe.

The sequences for the primers and probe used for monkey DMPK are 5′-AGCCTGAGCCGGGAGATG-3′ for the forward primer, 5′- GCGTAGTTGACTGGCAAAGTT-3′ for the reverse primer, and 5′-AGGCCATCCGCATGGCCAACC-3′ for the probe. Target RNA levels were normalized to cyclophilin mRNA expression. The sequences for the primers and probes used for cyclophilin A are 5′-CGACGGCGAGCCTTTG-3′ for the forward primer, 5′-TCTGCTGTCTTTGGAACCTTGTC-3′ for the reverse primer, and 5′-CGCGTCTCCTTCGAGCTGTTTGC-3′ for the probe.

Dose response curves were plotted using GraphPad Prizm 5 software. Data was fitted using the log(inhibitor) versus response – Variable slope (four parameters) option. For ED_{50} (dose which reduces the targeted mRNA by 50% relative to saline treated animals) calculations, the bottom and top were fixed to 0 and 100 respectively.

RESULTS

Palmitate, tocopherol and cholesterol enhance ASO association with albumin and lipoproteins and improve activity in extra-hepatic tissues in mice

We evaluated the plasma protein binding profile of palmitate, tocopherol and cholesterol ASO conjugates using a fluorescence polarization assay (Figure 1A). ASOs conjugated to all three hydrophobic moieties (Figure 1C) showed significant enhancements in binding affinity to albumin but binding to histidine-rich glycoprotein (HRG)—a high affinity PS ASO binding protein (28)—was largely unaltered (Figure 1B). Interestingly, all the ASO conjugates showed very significant enhancements in binding affinity for plasma lipoproteins (HDL and LDL) for which the parent ASO shows no affinity.

To determine if the differences in binding to the individual proteins is meaningful in plasma, we examined the plasma binding profile of the lipid-ASOs by size exclusion chromatography (Figure 1D). We also examined the effect of species and lipid on the binding profile as PS ASOs show different elution profiles when complexed with plasma from different species. PS ASOs coelute primarily with albumin in mouse, human and rat plasma whereas they coelute primarily with HRG in monkey plasma owing to the higher concentration of HRG in the monkey (28).

The palmitate ASO co-eluted with albumin/HRG for all the species evaluated. Very little free ASO was observed owing to the stronger interactions of palmitate-ASOs with albumin. The tocopherol-ASO showed a very broad elution profile and coeluted with the HDL and LDL fractions in plasma from all four species. The cholesterol ASO also showed a broad elution profile and was primarily associated with the HDL and LDL fractions in most species. A greater fraction of the cholesterol and tocopherol ASOs were associated with the LDL fractions in monkey and in human plasma, presumably because of the higher levels of LDL in primates as compared to rodents. Interestingly, greater fractions of the tocopherol and cholesterol conjugates were also associated with albumin in rat plasma because of the higher affinity of rat albumin for PS ASOs.

We determined if lipid-conjugation can enhance ASO activity in cells and in mice (Figure 1E). 3T3-L1 cells were differentiated in culture and treated with A-malat, Palm-

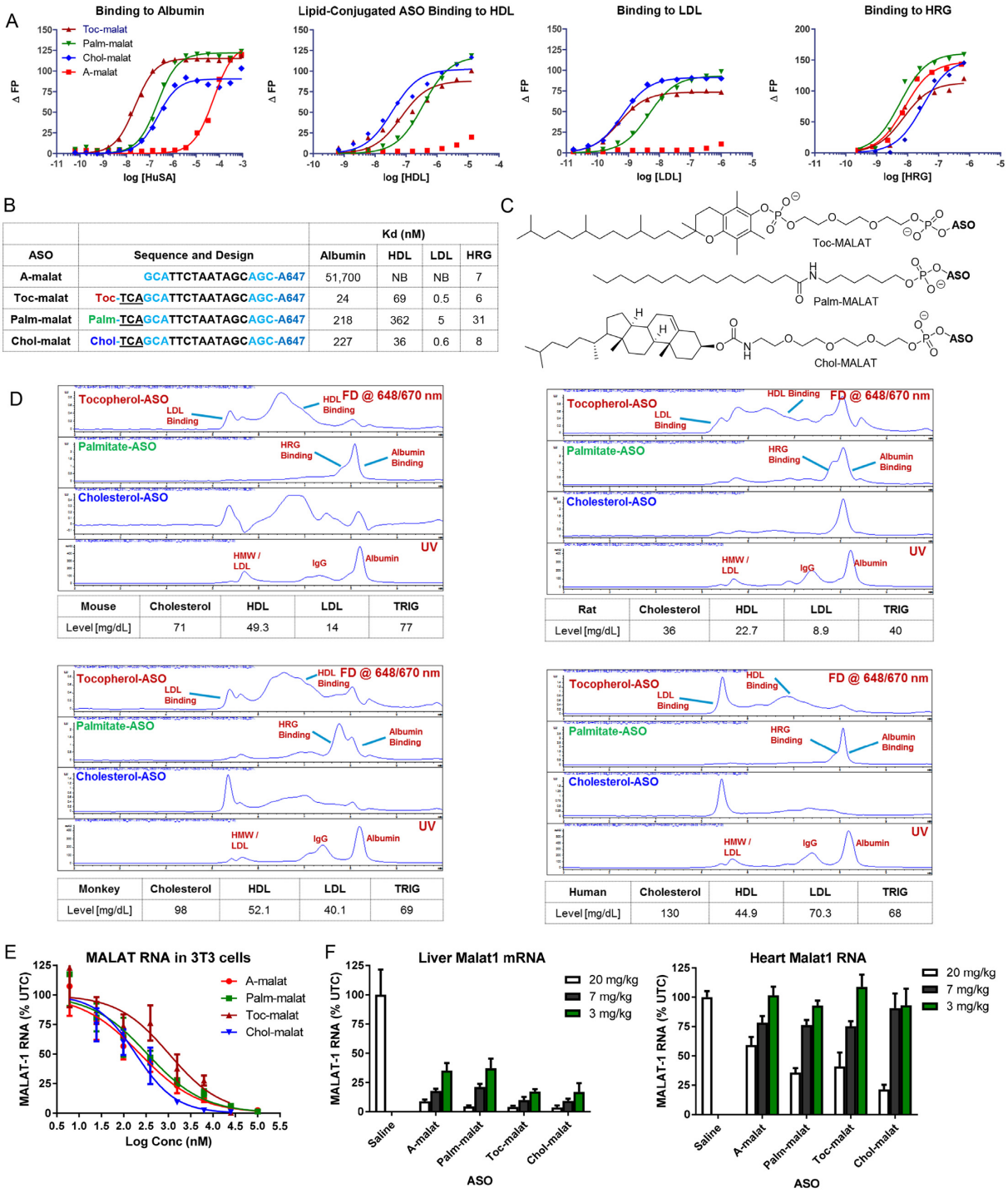

ASO	Sequence and Design	Kd (nM) Albumin	HDL	LDL	HRG
A-malat	GCATTCTAATAGCAGC-A647	51,700	NB	NB	7
Toc-malat	Toc-TCAGCATTCTAATAGCAGC-A647	24	69	0.5	6
Palm-malat	Palm-TCAGCATTCTAATAGCAGC-A647	218	362	5	31
Chol-malat	Chol-TCAGCATTCTAATAGCAGC-A647	227	36	0.6	8

Figure 1. Conjugation of hydrophobic moieties to PS ASOs modulates plasma protein binding and enhances activity in extra-hepatic tissues. (**A**) Binding curves and (**B**) dissociation constants of palmitate, tocopherol and cholesterol ASOs with albumin, HDL, LDL and HRG. NB = no binding (**C**) Structures of hydrophobic moieties conjugated to PS ASOs. Palm = palmitic acid, Toc = tocopherol, Chol = cholesterol, Blue = cEt and black = DNA nucleotides. (**D**) Comparison of protein binding profiles of palmitate, tocopherol and cholesterol conjugated PS ASOs in mouse, rat, monkey and human plasma by size exclusion chromatography. (E) All ASOs showed similar activity in 3T3-L1 cells for reducing MALAT-1 RNA when delivered by free uptake. (**F**) Conjugation of hydrophobic moieties enhances potency of a PS ASO gapmer targeting MALAT-1 RNA in the liver and heart. All errors are ±std. dev.

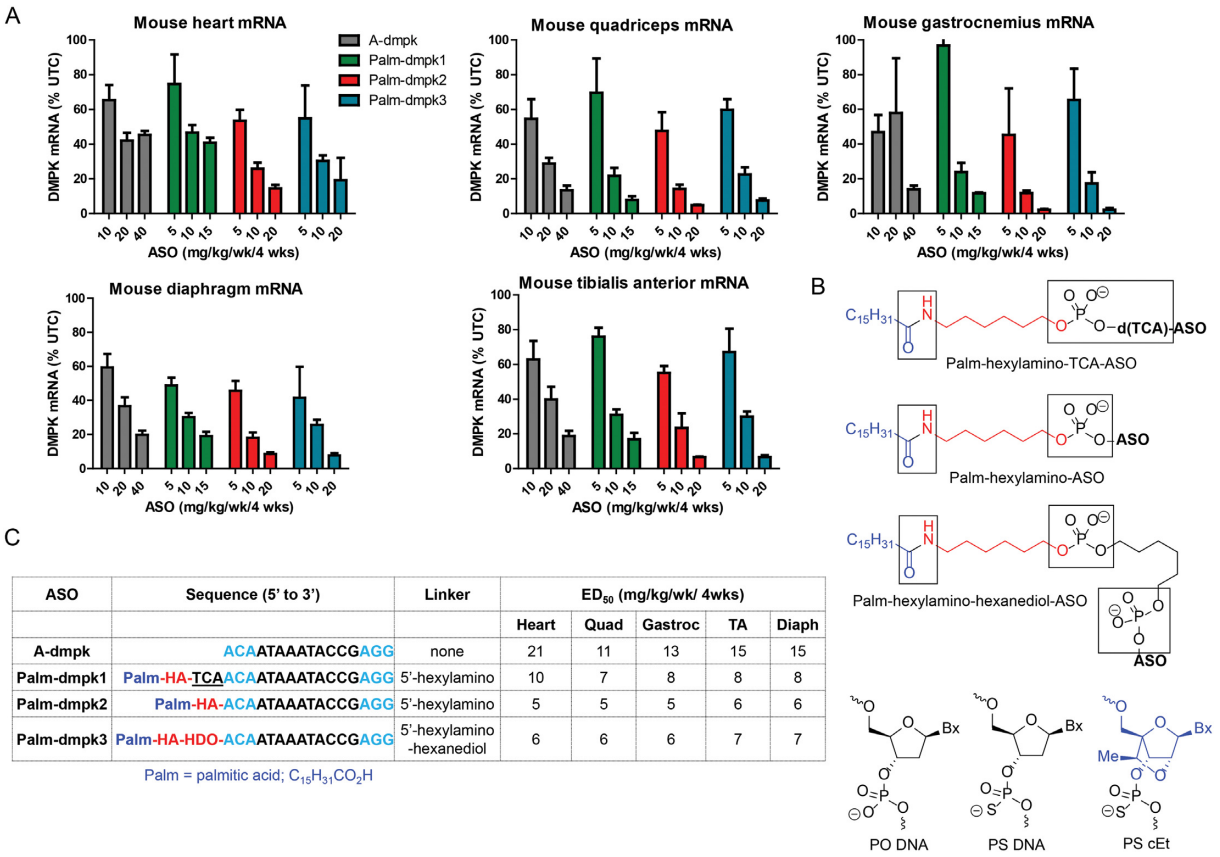

C

ASO	Sequence (5' to 3')	Linker	ED_{50} (mg/kg/wk/ 4wks)				
			Heart	Quad	Gastroc	TA	Diaph
A-dmpk	ACAATAAATACCGAGG	none	21	11	13	15	15
Palm-dmpk1	Palm-HA-TCAACAATAAATACCGAGG	5'-hexylamino	10	7	8	8	8
Palm-dmpk2	Palm-HA-ACAATAAATACCGAGG	5'-hexylamino	5	5	5	6	6
Palm-dmpk3	Palm-HA-HDO-ACAATAAATACCGAGG	5'-hexylamino -hexanediol	6	6	6	7	7

Palm = palmitic acid; $C_{15}H_{31}CO_2H$

Figure 2. Palmitate ASO-conjugates show enhanced potency in skeletal muscle and heart tissues in mice. (**A**) Mice (Balb-c mice, $n = 4$/group) were injected subcutaneously with 10, 20 or 40 mg/kg of A-dmpk, or with 5, 10 and 20 mg/kg of Palm-dmpk1, Palm-dmpk2 or Palm-dmpk3, once weekly for 4 weeks. Animals were sacrificed 48 hours after last injection and tissues were harvested. Reduction of DMPK mRNA in heart, quadriceps, gastrocnemius, tibialis anterior and diaphragm was quantified by qRT-PCR. (**B**) Structures and design of ASO conjugates tested. The boxed regions indicate potential sites of metabolic cleavage. (**C**) Dose required to reduce DMPK mRNA by 50% (ED_{50}) in various muscle tissues. Palm = palmitic acid, HA = hexylamino, HDO = 1,6-hexanediol, Blue = cEt and black = DNA nucleotides; All ASOs are full PS modified except underlined letters which are PO. All errors are ±std. dev.

malat, Toc-malat and Chol-malat ASOs by free uptake. All ASOs showed comparable potency for reducing MALAT-1 RNA expression as determined by qRT-PCR. Next, mice were intravenously injected once weekly for two weeks with 3, 10 or 20 mg/kg of ASO and sacrificed 48 hours after the last injection (Figure 1f and Supplementary Figure S2). Tissues were harvested and analyzed for reduction of MALAT-1 RNA by qRT-PCR. All the lipid conjugated ASOs showed improved activity in the heart while the Toc-malat and Chol-malat ASOs also showed slightly improved activity in the liver. These results showed that conjugating hydrophobic moieties enhances ASO activity in muscle tissues in mice but not in cells, suggesting that changes in tissue distribution may be responsible for the enhanced potency.

Palmitate conjugation enhances ASO potency in rodents

Given the species-dependent nature of interactions of PS ASOs with serum proteins, we first investigated if conjugation of palmitic acid (29) could enhance ASO activity in muscle tissues of rodents and monkeys. We performed our evaluations using an 3–10–3 cEt gapmer ASO A-dmpk, that is matched to mouse, rat, monkey and human dystrophia myotonica protein kinase (DMPK) mRNA (30). A toxic CTG repeat in the 3′-untranslated region of DMPK causes myotonic dystrophy (DM1), which is the most common form of muscular dystrophy in adults (31). The ASO conjugates were designed with three different linkers between the palmitate moiety and the ASO to facilitate ASO release after internalization into cells (Figure 2b). Palm-dmpk1 had an unmodified phosphodiester (PO)-trinucleotide linker and a hexylamino spacer to conjugate palmitate to the ASO. Palm-dmpk2 only had the hexylamino spacer, while Palm-dmpk3 had an additional hexanediol spacer. The additional spacers were hypothesized to facilitate ASO release from bound plasma proteins and/or lipoproteins which could be internalized along with the tightly bound ASO.

Mice were injected subcutaneously once weekly for four weeks with 10, 20, 40 mg/kg of A-dmpk or 5, 10 and 20 mg/kg of Palm-dmpk1, Palm-dmpk2 and Palm-dmpk3. Animals were sacrificed 48 hours after the last dose and heart, quadriceps, tibialis anterior, diaphragm and gastrocnemius muscle tissues were harvested to assess knockdown of DMPK mRNA by qRT-PCR. The dose required to reduce DMPK mRNA in all tissues by 50% was calculated using a non-linear regression fit. ASO A-dmpk showed dose-

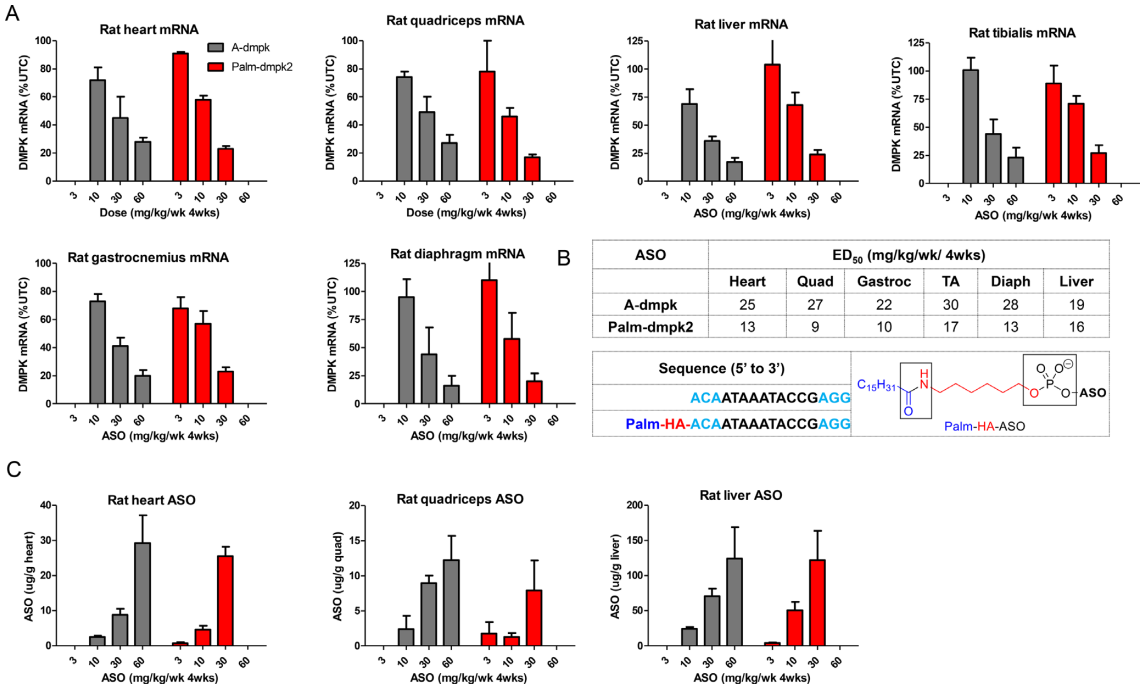

Figure 3. Palmitate ASO-conjugates show enhanced potency in skeletal muscle and heart tissues in rats. (**A**) Rats (SD, $n = 4$/group) were injected subcutaneously with 10, 30 or 60 mg/kg of A-dmpk, or with 3, 10 and 30 mg/kg of Palm-dmpk2, once weekly for 4 weeks. Animals were sacrificed 48 h after last injection and tissues were harvested. Reduction of DMPK mRNA in heart, quadriceps, liver, gastrocnemius, tibialis anterior and diaphragm was quantified by qRT-PCR. (**B**) Structures, sequence, design of ASO conjugates and ED_{50} (mg/kg) in various muscle tissues. Palm = palmitic acid, HA = hexylamino, Blue = cEt and black = DNA nucleotides; All ASOs are full PS modified. (**C**) ASO accumulation in the heart, quadriceps and liver as determined by LCMS. All errors are ±std. dev.

dependent reductions of DMPK mRNA in all muscle tissues investigated with ED_{50} values ranging from 11 to 21 mg/kg (Figure 2A and C). In contrast, all the palmitate ASOs showed 2–3-fold enhancements in potency. All ASO conjugates were well tolerated with no overt toxicities (Supplementary Figure S3). The best results were observed with Palm-dmpk2 which has a hexylamino spacer between the ASO and the palmitic acid. This linking strategy is similar to that used for several GalNAc–ASO conjugates in clinical development (32). Given the performance of this ASO, the rest of the evaluations in rat and monkey were performed using Palm-dmpk2.

We determined if Palm-dmpk2 could enhance ASO activity in rats. Rats were subcutaneously injected once weekly for four weeks with 10, 30 and 60 mg/kg of A-dmpk or 3, 10 and 30 mg/kg of Palm-dmpk2. The animals were sacrificed 48 hours following the last dose and organs were harvested to assess DMPK mRNA reduction by qRT-PCR. In general, both ASOs were well tolerated with no obvious toxicities or alterations in blood chemistries or organ weights (Supplementary Figure S4). Both ASOs showed dose dependent knockdown of DMPK mRNA in the liver, heart and quadriceps and the Palm-dmpk2 showed 2–3-fold improved activity relative to A-dmpk in all tissues evaluated (Figure 3A and B). We also evaluated tissue concentrations for both ASOs in liver and muscle tissues and observed dose-dependent increases in ASO accumulation (Figure 3C). Modest improvements in ASO accumulation in the liver and the heart were observed in rats treated with Palm-dmpk2 relative to A-dmpk.

Palmitate conjugation modestly enhances ASO activity in monkeys

We determined if Palm-dmpk2 could enhance ASO activity in monkeys. Cynomolgus monkeys were subcutaneously injected with 10 doses of 10, 20 and 40 mg/kg of A-dmpk or Palm-dmpk2 over 7 weeks (Figure 4A). Animals were sacrificed 48 hours after the last dose and organs were harvested to assess DMPK mRNA reduction by qRT-PCR. As seen in the rat study, both ASOs were well tolerated with no obvious toxicities or alterations in blood chemistries (Supplementary Figure S5). Both ASOs showed a dose-dependent reduction of DMPK mRNA in the heart and the quadriceps (Figure 4B). It was difficult to assess the reduction of DMPK mRNA in the liver because of low abundance of transcript in this tissue. In general, we observed a modest improvement in potency (ED_{50}) in most muscle tissues evaluated (Figure 4C). However, an improvement in efficacy (maximal target reduction) was observed in muscle tissues for animals treated with 40 mg/kg of Palm-dmpk2.

Similar levels of ASO accumulation in the liver, tibialis anterior and quadriceps for all dose levels were observed (Figure 4D). The major metabolite extracted from tissues for animals treated with Palm-dmpk2 was the parent ASO A-dmpk suggesting that the palmitate and the hexylamino moieties were cleaved from the conjugate by metabolism after internalization into tissues. Modest improvements in ASO accumulation in the heart was observed for the 20 and 40 mg/kg Palm-dmpk2 treated dose-groups. While we did not observe substantial improvements in ASO potency with

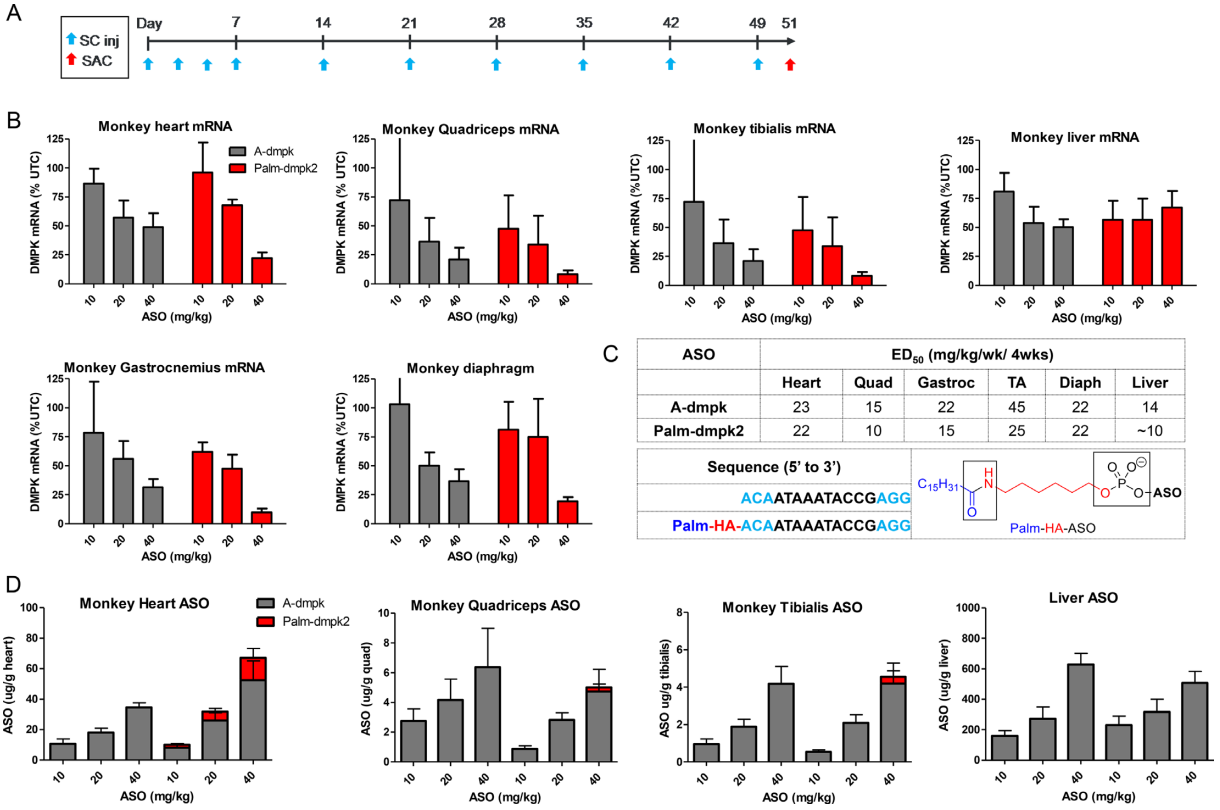

Figure 4. Palmitate ASO-conjugates show enhanced efficacy in skeletal muscle and heart tissues in monkeys. (**A**) Dosing frequency and schedule for ASO injections. (**B**) Cynomolgus monkeys ($n = 4$/group) were injected subcutaneously with 10 injections over 7 weeks of 10, 20 or 40 mg/kg of A-dmpk or Palm-dmpk2. Animals were sacrificed 48 hours after last injection and tissues were harvested. Reduction of DMPK mRNA in heart, quadriceps, liver, gastrocnemius, tibialis anterior and diaphragm was quantified by qRT-PCR. (**C**) Structures, sequence, design of ASO conjugates and ED_{50} (mg/kg) in various muscle tissues. Palm = palmitic acid, HA = hexylamino, Blue = cEt and black = DNA nucleotides; All ASOs are full PS modified. (**D**) ASO accumulation in the heart, quadriceps, tibialis anterior and liver as determined by LCMS. For Palm-dmpk2, the majority of conjugate was metabolized in tissues to liberate A-dmpk. All errors are ±std. dev.

palmitate conjugation in the monkey, Palm-dmpk2 showed improved efficacy relative to A-dmpk in all muscle tissues evaluated with close to 90% mRNA knockdown observed in some muscle tissues.

Tocopherol and cholesterol conjugation enhance ASO potency in the muscle but cholesterol ASOs are toxic at higher doses

Given the results with palmitate ASO in the monkey, we determined if tocopherol or cholesterol could be more useful for enhancing ASO potency in the monkey. All ASO conjugates were evaluated with phosphodiester (PO) trinucleotide-spacer between the lipid and the ASO (Figure 5B) (33). Previous work has shown that these type linkers are stable in plasma but rapidly metabolized in endolysosomal compartments after internalization into cells (34). We first evaluated the optimal mode of injection for administration of tocopherol and cholesterol ASO conjugates. Mice were injected subcutaneously or intravenously once weekly for four weeks with a single injection of 10 mg/kg of Toc-dmpk, Chol-dmpk or Palm-dmpk2. Animals were sacrificed 48 hours after the last injection and tissues were harvested and analyzed for reduction of DMPK mRNA by qRT-PCR. All ASOs were well tolerated (Supplementary Figure S6). Toc-dmpk and Chol-dmpk ASOs showed significantly improved potency when delivered by intravenous injection (Figure 5A). In contrast, Palm-dmpk2 was almost as active when delivered by subcutaneous or intravenous injection. It is conceivable that the more hydrophobic nature of tocopherol and cholesterol causes the ASO to be sequestered and released less efficiently from the injection site following subcutaneous administration.

We next evaluated the effect of tocopherol and cholesterol conjugation on potency in the skeletal muscle and heart using mice in a multiple dosing regimen. Mice were injected intravenously once weekly for four weeks with 5, 10 and 20 mg/kg of the parent ASO A-dmpk or the conjugates Toc-dmpk or Chol-dmpk respectively. The animals were sacrificed 48 hours after the last dose and tissues were harvested to quantify DMPK mRNA reduction by qRT-PCR. The parent ASO A-dmpk and the tocopherol conjugate Toc-dmpk were well tolerated at all doses tested (Supplementary Figure S7). However, the cholesterol ASO was toxic at 20 mg/kg dose and resulted in mortality. Both, Toc-dmpk and Chol-dmpk, showed enhanced potency relative to A-dmpk in the heart, quadriceps and in tibialis anterior muscles (Figure 5C and D). Chol-dmpk showed the best potency enhancement in muscle but this ASO was not ad-

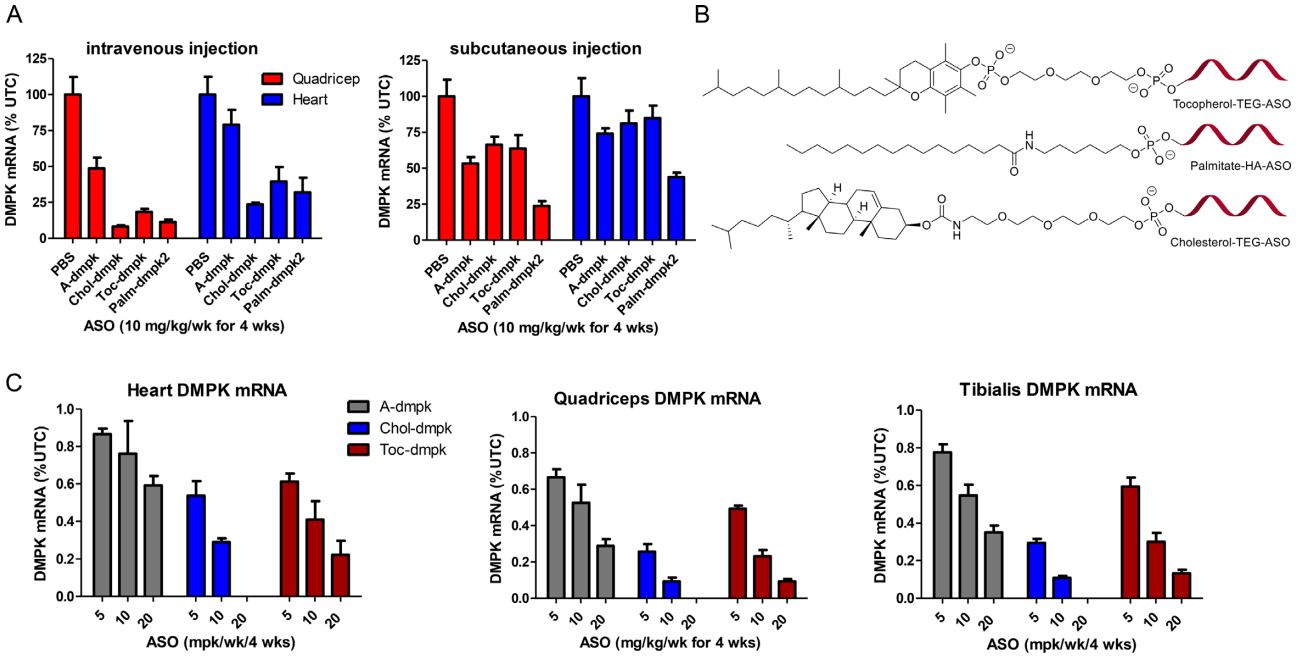

D

ASO	Sequence (5'-3')	5'-conjugate (X)	ED_{50} (mg/kg)		
			heart	quad	TA
A-dmpk	ACAATAAATACCGAGG	none	24	15	14
Chol-dmpk	X-TCAACAATAAATACCGAGG	Cholesterol-TEG	5	4	4
Toc-dmpk	X-TCAACAATAAATACCGAGG	Tocopherol-TEG	7	7	7

Figure 5. Palmitate, tocopherol and cholesterol conjugation enhances ASO activity in quadriceps and heart tissues. (**A**) Comparison of ASO activity in quadriceps and heart after a single subcutaneous or intravenous injection of ASO-conjugates. Mice (Balb-c, $n = 4$/group) were injected once weekly for four weeks with 10 mg/kg of A-dmpk, Palm-dmpk2, Toc-dmpk or Chol-dmpk. Animals were sacrificed 48 h after the last dose and DMPK mRNA reduction in quadriceps and heart was determined using qRT-PCR. (**B**) Structures of ASO conjugates. (**C**) Comparison of ASO activity in quadriceps and heart after four intravenous injection of ASO-conjugates. Mice (Balb-c, $n = 4$/group) were injected once weekly for 4 weeks with 5, 10 or 20 mg/kg of A-dmpk, Toc-dmpk or Chol-dmpk. Animals were sacrificed 48 h after the last dose and DMPK mRNA reduction in heart, quadriceps and tibialis anterior was determined using qRT-PCR. (**D**) Sequence and design of ASO conjugates and ED_{50} (mg/kg) in various muscle tissues. Palm = palmitic acid, Toc = tocopherol, Chol = cholesterol, HA = hexylamino, Blue = cEt and black = DNA nucleotides; All ASOs are full PS modified except the underlined nucleotides which are PO. All errors are ±std. dev.

vanced any further owing to the toxicity observed at the 20 mg/kg dose.

Tocopherol conjugation enhances ASO potency in the monkey

Toc-dmpk was evaluated in the monkey to determine if changes in plasma protein binding observed with tocopherol-ASO conjugates would translate to improved potency. Cynomolgus monkeys were injected intravenously with 10 injections of A-dmpk at 20 and 40 mg/kg, or with Toc-dmpk at 10, 20 and 40 mg/kg over 7 weeks (Figure 6A). The animals were sacrificed 48 hours after the last dose and tissues were harvested to determine reductions in DMPK mRNA by qRT-PCR. Both ASOs were generally well tolerated with no significant changes in plasma chemistries or organ weights (Supplementary Figure S8). Both ASO showed dose-dependent reductions in DMPK mRNA in the heart, quadriceps and gastrocnemius but Toc-dmpk was slightly more potent (Figure 6B and C). Toc-dmpk showed slight enhancements in ASO accumulation in the liver and heart and similar ASO accumulation in quadriceps (Figure 6D). Slightly reduced ASO accumulation in the kidney relative to A-dmpk was observed as enhancing association with plasma lipoproteins reduces exposure of oligonucleotide drugs to the kidney. Unlike the palmitate conjugate Palm-dmpk2 which was almost completely metabolized to A-dmpk in tissues, the majority of the ASO extracted from tissues for Toc-dmpk was the parent tocopherol-conjugated ASO (Figure 6D). It is possible that the tocopherol-moiety of Toc-dmpk inserts into lipoprotein particles and impedes access of cellular nucleases to the cleavable PO d(TCA) linker. This could result in slower metabolism of Toc-dmpk to release A-dmpk in tissues and any potential effects this could have on ASO activity remain unclear.

DISCUSSION

Several muscle diseases arise from aberrations in mRNA splicing or from accumulation of toxic RNA which make them uniquely suited for antisense intervention (7,8). PS ASOs can be delivered effectively to muscle tissues in rodents after systemic injection, but doses required to elicit antisense pharmacology are higher than those required in the liver (13). This can result in dose-limiting toxicities in the clinic. While significant advances have been made to iden-

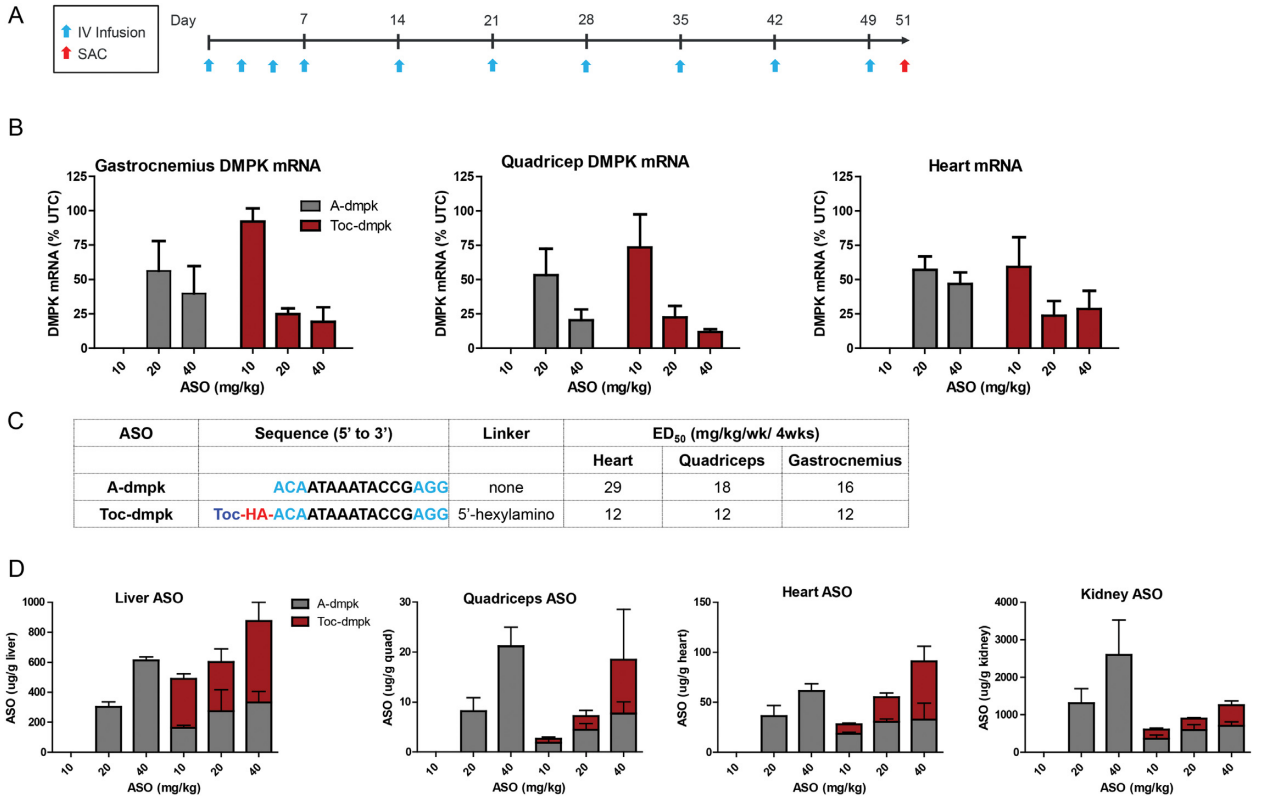

ASO	Sequence (5' to 3')	Linker	ED_{50} (mg/kg/wk/ 4wks)		
			Heart	Quadriceps	Gastrocnemius
A-dmpk	ACAATAAATACCGAGG	none	29	18	16
Toc-dmpk	Toc-HA-ACAATAAATACCGAGG	5'-hexylamino	12	12	12

Figure 6. Tocopherol ASO-conjugates show enhanced activity in skeletal muscle and heart tissues in monkeys. (**A**) Dosing frequency and schedule for ASO injections. (**B**) Cynomolgus monkeys ($n = 4$/group) were injected intravenously with 10 injections over 7 weeks of 10, 20 or 40 mg/kg of A-dmpk or Toc-dmpk. Animals were sacrificed 48 hours after last injection and tissues were harvested. Reduction of DMPK mRNA in heart, quadriceps, gastrocnemius was quantified by qRT-PCR. (**C**) Sequence and design of ASO conjugates and ED_{50} (mg/kg) in various muscle tissues. Toc = tocopherol, HA = hexylamino, Blue = cEt and black = DNA nucleotides; All ASOs are full PS modified except the underlined nucleotides which are PO. (**D**) ASO accumulation in the heart, quadriceps and liver as determined by AEX. For Toc-dmpk, the majority of the ASO extracted from tissues was the intact parent conjugate-ASO. All errors are ±std. dev.

tify ASO designs to increase intrinsic potency (35), identifying strategies to enhance ASO activity in muscle tissues is important for treating muscle diseases using nucleic acid-based therapeutic agents.

Chemically modified single stranded PS ASOs are highly protein-bound in plasma which facilitates distribution to peripheral tissues from the site of injection (36). PS ASOs distribute broadly to several cell-types and tissues after systemic injection but accumulate preferentially in the liver, kidney, spleen and bone-marrow in animals (37). Higher accumulation in these tissues can be attributed to expression of stabilin receptors on endothelial cells (38) and to the porous vasculature which allows macromolecular therapeutics such as ASOs to exit the blood compartment and be taken up into parenchymal cells (39). However, unlike the sinusoidal and fenestrated capillaries in the liver and the kidneys, muscle tissues have a continuous endothelium which represents a significant tissue barrier that must be overcome for effective delivery to muscle cells (16).

Plasma proteins such as albumin and lipoproteins are readily transported across the capillary endothelium by caveolin-mediated transcytosis (40). Indeed, almost 60% of total albumin is extra vascular and resides in the interstitial spaces of muscle, skin and adipose tissues (18). Albumin is estimated to make ∼28 trips in and out of the lymphatic system during its lifetime as it shuttles between the extravascular space and the blood compartment (19). Thus, enhancing association with plasma proteins such as albumin and lipoproteins represents one strategy to enhance delivery of macromolecular therapeutics to the muscle.

PS ASOs associate primarily with albumin in plasma with relatively modest affinity (K_d = 10–50 μM). The association of PS ASOs with albumin and lipoproteins can be augmented by conjugation of hydrophobic moieties such as cholesterol, fatty acids and fat-soluble vitamins (20,41). PS ASOs also interact differently with plasma proteins from different species and this can facilitate or impede ASO delivery to specific cell-types and tissues in a species-dependent manner (42). Given this background, we investigated the effect of conjugating hydrophobic moieties to PS ASOs on enhancing ASO potency in muscle tissues in mice, rat and monkey – the three most commonly used species for preclinical evaluation of ASO therapeutics.

Palmitate conjugated ASOs showed good potency enhancement in skeletal muscle and heart in mice and in rats. However, this design was less effective for enhancing ASO potency in the monkey. To determine if other hydrophobic moieties such as tocopherol or cholesterol could enhance ASO potency in the monkey, we first evaluated these conjugates in mice. Both hydrophobes enhanced ASO po-

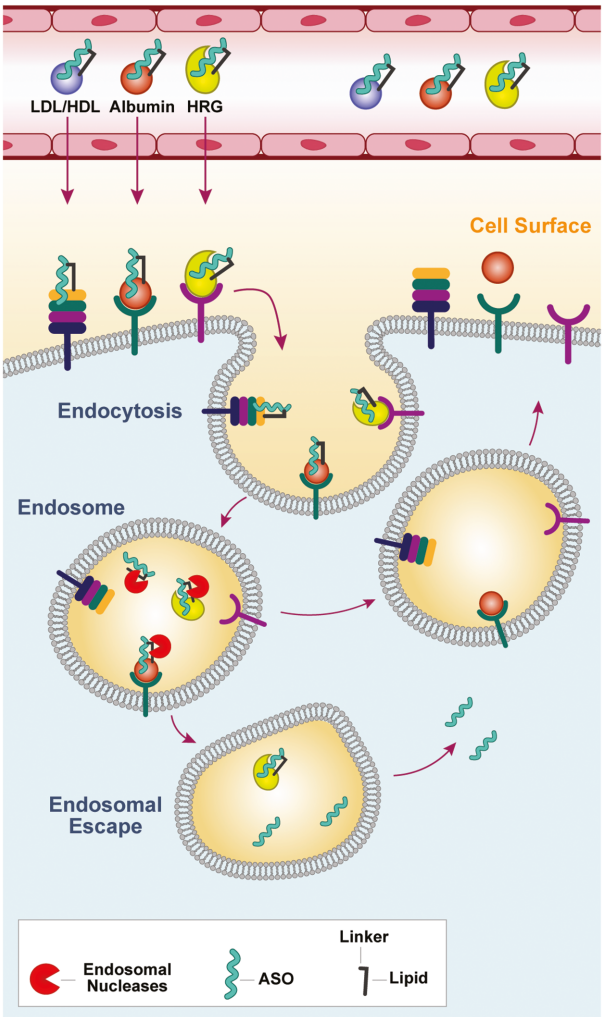

Figure 7. A potential model to rationalize how modulating interactions with plasma proteins by conjugating hydrophobic moieties can enhance ASO potency in muscle tissues. Lipid conjugation enhances affinity for plasma proteins which facilitates transport across the capillary endothelium. The lipid-ASOs partition onto protein acceptors on the cell surface or are internalized as ASO-protein complexes and transported to late endosomal compartments. Cleavage of the linker between the ASO and the lipid by endosomal nucleases can facilitate ASO release from proteins such as albumin and lipoproteins for which PS-ASOs have lower affinity. However, PS-ASOs can stay bound to higher-affinity proteins such as HRG and this may hinder ASO escape from endosomal compartments.

tency in the muscle and optimal effects were seen with cholesterol conjugation. Unfortunately, this approach also showed higher toxicity and was not advanced into the monkey. Tocopherol ASO conjugates showed 2-fold enhanced potency in the monkey and also showed modest enhancements in tissue accumulation. However, tocopherol ASO conjugates show best activity when delivered by intravenous injections which can decrease patient convenience, especially for disease indications that require life time therapy. In contrast, the palmitate conjugates are almost equally active in rodents when delivered by more convenient subcutaneous injections but less effective at enhancing ASO potency in monkeys.

The modest potency improvement observed with palmitate ASOs in the monkey is perplexing and represents one of many pitfalls associated with real life drug discovery where species-dependent effects can impose significant obstacles. We recently showed that proteins which binding PS ASOs with high affinity such as μ-2-macroglobin and HRG can reduce ASO activity in mice (28,43). One possible explanation for the modest potency enhancement in the monkey could be that the ASO is internalized into endo-lysosomal compartments in cells as a tight complex with proteins such as HRG which are present at higher concentrations in monkey plasma (Figure 7). Indeed, PS ASOs generally show reduced activity in the monkey even for gene targets expressed in the liver. This could impede ASO escape from endo-lysosomal compartments which is an absolute requirement for antisense activity. Alternatively, the tightly bound lipid ASO–protein complexes are not as efficient at being transcytosed and get sequestered within endothelial cells where the ASO is intrinsically less active (44). It should be noted that GalNac-ASO conjugates which showed 7–10-fold improved potency in rodents (4), were found to be 30-fold more potent than their unconjugated counterparts in humans (5). Extrapolation of these results would suggest that lipid-ASOs could exhibit significant improvement in potency enhancement in man. Furthermore, monkey may not a good predictor for activity of lipid ASOs in man given that the plasma protein binding profile of PS ASOs in man resembles mouse more closely than monkey.

In conclusion, we show that enhancing association with plasma proteins can enhance ASO potency in the skeletal muscle and heart of rodents and monkeys. The lipid ASO conjugates were well tolerated in general with the exception of the single stranded cholesterol ASO conjugates which were toxic at higher doses. Modulating interactions with plasma proteins to facilitate tissue distribution represents an example of passive targeting (16). It is conceivable that the efficiency of this approach can be further improved by conjugating lipid ASOs to ligands which target cell-surface receptors in muscle tissues. Our work lays the foundation for developing more effective strategies for targeting muscle tissues with PS ASOs in order to deliver disease-modifying treatments to patients.

SUPPLEMENTARY DATA

Supplementary Data are available at NAR Online.

FUNDING

Ionis Pharmaceuticals. Funding for open access charge: Ionis Pharmaceuticals.
Conflict of interest statement. None declared.

REFERENCES

1. Crooke,S.T., Witztum,J.L., Bennett,C.F. and Baker,B.F. (2018) RNA-Targeted therapeutics. *Cell Metab.*, **27**, 714–739.
2. Eckstein,F. (2014) Phosphorothioates, essential components of therapeutic oligonucleotides. *Nucleic Acid Ther.*, **24**, 374–387.
3. Crooke,S.T., Wang,S., Vickers,T.A., Shen,W. and Liang,X-h. (2017) Cellular uptake and trafficking of antisense oligonucleotides. *Nat. Biotech.*, **35**, 230–237.

4. Prakash,T.P., Graham,M.J., Yu,J., Carty,R., Low,A., Chappell,A., Schmidt,K., Zhao,C., Aghajan,M., Murray,H.F. *et al.* (2014) Targeted delivery of antisense oligonucleotides to hepatocytes using triantennary N-acetyl galactosamine improves potency 10-fold in mice. *Nucleic Acids Res.*, **42**, 8796–8807.
5. Crooke,S.T., Baker,B.F., Xia,S., Yu,R.Z., Viney,N.J., Wang,Y., Tsimikas,S. and Geary,R.S. (2019) Integrated assessment of the clinical performance of GalNAc3-Conjugated 2′-O-Methoxyethyl chimeric antisense oligonucleotides: I.Human Volunteer Experience. *Nucleic Acid Ther.*, **29**, 16–32.
6. Ämmälä,C., Drury,W.J., Knerr,L., Ahlstedt,I., Stillemark-Billton,P., Wennberg-Huldt,C., Andersson,E.-M., Valeur,E., Jansson-Löfmark,R., Janzén,D. *et al.* (2018) Targeted delivery of antisense oligonucleotides to pancreatic β-cells. *Sci. Adv.*, **4**, eaat3386.
7. Spitali,P. and Aartsma-Rus,A. (2012) Splice modulating therapies for human disease. *Cell*, **148**, 1085–1088.
8. Thornton,C.A., Wang,E. and Carrell,E.M. (2017) Myotonic dystrophy: approach to therapy. *Curr. Opin. Genet. Dev.*, **44**, 135–140.
9. Bennett,C.F. and Swayze,E.E. (2010) RNA targeting therapeutics: molecular mechanisms of antisense oligonucleotides as a therapeutic platform. *Annu. Rev. Pharmacol. Toxicol.*, **50**, 259–293.
10. Voit,T., Topaloglu,H., Straub,V., Muntoni,F., Deconinck,N., Campion,G., De Kimpe,S.J., Eagle,M., Guglieri,M., Hood,S. *et al.* (2014) Safety and efficacy of drisapersen for the treatment of Duchenne muscular dystrophy (DEMAND II): an exploratory, randomised, placebo-controlled phase 2 study. *Lancet Neurol.*, **13**, 987–996.
11. Tasfaout,H., Buono,S., Guo,S., Kretz,C., Messaddeq,N., Booten,S., Greenlee,S., Monia,B.P., Cowling,B.S. and Laporte,J. (2017) Antisense oligonucleotide-mediated Dnm2 knockdown prevents and reverts myotubular myopathy in mice. *Nat. Commun.*, **8**, 15661.
12. Lieberman,A.P., Yu,Z., Murray,S., Peralta,R., Low,A., Guo,S., Yu,X.X., Cortes,C.J., Bennett,C.F., Monia,B.P. *et al.* (2014) Peripheral androgen receptor gene suppression rescues disease in mouse models of spinal and bulbar muscular atrophy. *Cell Rep.*, **7**, 774–784.
13. Murray,S., Ittig,D., Koller,E., Berdeja,A., Chappell,A., Prakash,T.P., Norrbom,M., Swayze,E.E., Leumann,C.J. and Seth,P.P. (2012) TricycloDNA-modified oligo-2′-deoxyribonucleotides reduce scavenger receptor B1 mRNA in hepatic and extra-hepatic tissues–a comparative study of oligonucleotide length, design and chemistry. *Nucleic Acids Res.*, **40**, 6135–6143.
14. Goemans,N.M., Tulinius,M., van den Hauwe,M., Kroksmark,A.K., Buyse,G., Wilson,R.J., van Deutekom,J.C., de Kimpe,S.J., Lourbakos,A. and Campion,G. (2016) Long-Term efficacy, safety, and pharmacokinetics of drisapersen in duchenne muscular dystrophy: Results from an Open-Label extension study. *PLoS One*, **11**, e0161955.
15. Geary,R.S., Norris,D., Yu,R. and Bennett,C.F. (2015) Pharmacokinetics, biodistribution and cell uptake of antisense oligonucleotides. *Adv. Drug Delivery Rev.*, **87**, 46–51.
16. Seth,P.P., Tanowitz,M. and Bennett,C.F. (2019) Selective tissue targeting of synthetic nucleic acid drugs. *J. Clin. Invest.*, **129**, 915–925.
17. Simionescu,M., Gafencu,A. and Antohe,F. (2002) Transcytosis of plasma macromolecules in endothelial cells: A cell biological survey. *Microsc. Res. Tech.*, **57**, 269–288.
18. Ellmerer,M., Schaupp,L., Brunner,G.A., Sendlhofer,G., Wutte,A., Wach,P. and Pieber,T.R. (2000) Measurement of interstitial albumin in human skeletal muscle and adipose tissue by open-flow microperfusion. *Am. J. Physiol. - Endocrinol. Metab.*, **278**, E352–E356.
19. Merlot,A.M., Kalinowski,D.S. and Richardson,D.R. (2014) Unraveling the mysteries of serum albumin – more than just a serum protein. *Front. Physiol.*, **5**, 299.
20. Crooke,S.T., Graham,M.J., Zuckerman,J.E., Brooks,D., Conklin,B.S., Cummins,L.L., Greig,M.J., Guinosso,C.J., Kornbrust,D., Manoharan,M. *et al.* (1996) Pharmacokinetic properties of several novel oligonucleotide analogs in mice. *J. Pharmacol. Exp. Ther.*, **277**, 923–937.
21. Wolfrum,C., Shi,S., Jayaprakash,K.N., Jayaraman,M., Wang,G., Pandey,R.K., Rajeev,K.G., Nakayama,T., Charrise,K., Ndungo,E.M. *et al.* (2007) Mechanisms and optimization of in vivo delivery of lipophilic siRNAs. *Nat. Biotechnol.*, **25**, 1149–1157.
22. Osborn,M.F., Coles,A.H., Biscans,A., Haraszti,R.A., Roux,L., Davis,S., Ly,S., Echeverria,D., Hassler,M.R., Godinho,B.M.D.C. *et al.* (2018) Hydrophobicity drives the systemic distribution of lipid-conjugated siRNAs via lipid transport pathways. *Nucleic Acids Res.*, **47**, 1070–1081.
23. Biscans,A., Coles,A., Haraszti,R., Echeverria,D., Hassler,M., Osborn,M. and Khvorova,A. (2018) Diverse lipid conjugates for functional extra-hepatic siRNA delivery in vivo. *Nucleic Acids Res.*, **47**, 1082–1096.
24. Khan,T., Weber,H., DiMuzio,J., Matter,A., Dogdas,B., Shah,T., Thankappan,A., Disa,J., Jadhav,V., Lubbers,L. *et al.* (2016) Silencing myostatin using Cholesterol-conjugated siRNAs induces muscle growth. *Mol. Ther Nucleic Acids*, **5**, e342.
25. Moroz,E., Lee,S.H., Yamada,K., Halloy,F., Martínez-Montero,S., Jahns,H., Hall,J., Damha,M.J., Castagner,B. and Leroux,J.-C. (2016) Carrier-free gene silencing by amphiphilic nucleic acid conjugates in differentiated intestinal cells. *Mol. Ther. Nucleic Acids*, **5**, e364.
26. Biscans,A., Coles,A., Echeverria,D. and Khvorova,A. (2019) The valency of fatty acid conjugates impacts siRNA pharmacokinetics, distribution, and efficacy in vivo. *J. Control Release*, **302**, 116–125.
27. Nishina,K., Piao,W., Yoshida-Tanaka,K., Sujino,Y., Nishina,T., Yamamoto,T., Nitta,K., Yoshioka,K., Kuwahara,H., Yasuhara,H. *et al.* (2015) DNA/RNA heteroduplex oligonucleotide for highly efficient gene silencing. *Nat. Commun.*, **6**, 7969.
28. Gaus,H.J., Gupta,R., Chappell,A.E., Østergaard,M.E., Swayze,E.E. and Seth,P.P. (2018) Characterization of the interactions of chemically-modified therapeutic nucleic acids with plasma proteins using a fluorescence polarization assay. *Nucleic Acids Res.*, **47**, 1110–1122.
29. Prakash,T.P., Mullick,A.E., Lee,R.G., Yu,J., Yeh,S.T., Low,A., Chappell,A.E., Oestergaard,M.E., Murray,S., Gaus,H.J. *et al.* (2019) Fatty acid conjugation enhances potency of antisense oligonucleotides in muscle. *Nucleic Acids Res.*, doi:10.1093/nar/gkz354.
30. Pandey,S.K., Wheeler,T.M., Justice,S.L., Kim,A., Younis,H.S., Gattis,D., Jauvin,D., Puymirat,J., Swayze,E.E., Freier,S.M. *et al.* (2015) Identification and characterization of modified antisense oligonucleotides targeting DMPK in mice and nonhuman primates for the treatment of myotonic dystrophy type 1. *J. Pharmacol. Exp. Ther.*, **355**, 329–340.
31. Wheeler,T.M., Leger,A.J., Pandey,S.K., MacLeod,A.R., Nakamori,M., Cheng,S.H., Wentworth,B.M., Bennett,C.F. and Thornton,C.A. (2012) Targeting nuclear RNA for in vivo correction of myotonic dystrophy. *Nature*, **488**, 111–115.
32. Prakash,T.P., Yu,J., Migawa,M.T., Kinberger,G.A., Wan,W.B., Ostergaard,M.E., Carty,R.L., Vasquez,G., Low,A., Chappell,A. *et al.* (2016) Comprehensive Structure-Activity relationship of triantennary N-Acetylgalactosamine conjugated antisense oligonucleotides for targeted delivery to hepatocytes. *J. Med. Chem.*, **59**, 2718–2733.
33. Nishina,T., Numata,J., Nishina,K., Yoshida-Tanaka,K., Nitta,K., Piao,W., Iwata,R., Ito,S., Kuwahara,H., Wada,T. *et al.* (2015) Chimeric antisense oligonucleotide conjugated to [alpha]-Tocopherol. *Mol. Ther. Nucleic Acids*, **4**, e220.
34. Ostergaard,M.E., Yu,J., Kinberger,G.A., Wan,W.B., Migawa,M.T., Vasquez,G., Schmidt,K., Gaus,H.J., Murray,H.M., Low,A. *et al.* (2015) Efficient synthesis and biological evaluation of 5′-GalNAc conjugated antisense oligonucleotides. *Bioconjug. Chem.*, **26**, 1451–1455.
35. Wan,W.B. and Seth,P.P. (2016) The medicinal chemistry of therapeutic oligonucleotides. *J. Med. Chem.*, **59**, 9645–9667.
36. Geary,R.S., Yu,R.Z. and Levin,A.A. (2001) Pharmacokinetics of phosphorothioate antisense oligodeoxynucleotides. *Curr. Opin. Investig. Drugs*, **2**, 562–573.
37. Yu,R.Z., Kim,T.-W., Hong,A., Watanabe,T.A., Gaus,H.J. and Geary,R.S. (2007) Cross-Species pharmacokinetic comparison from mouse to man of a Second-Generation antisense oligonucleotide, ISIS 301012, targeting human apolipoprotein B-100. *Drug Metab. Dispos*, **35**, 460–468.
38. Miller,C.M., Donner,A.J., Blank,E.E., Egger,A.W., Kellar,B.M., Ostergaard,M.E., Seth,P.P. and Harris,E.N. (2016) Stabilin-1 and Stabilin-2 are specific receptors for the cellular internalization of phosphorothioate-modified antisense oligonucleotides (ASOs) in the liver. *Nucleic Acids Res.*, **44**, 2782–2794.

39. Miller,C.M., Tanowitz,M., Donner,A.J., Prakash,T.P., Swayze,E.E., Harris,E.N. and Seth,P.P. (2018) Receptor-Mediated uptake of phosphorothioate antisense oligonucleotides in different cell types of the liver. *Nucleic Acid Ther.*, **28**, 119–127.
40. Schnitzer,J.E. (2001) Caveolae: from basic trafficking mechanisms to targeting transcytosis for tissue-specific drug and gene delivery in vivo. *Adv. Drug Deliv. Rev*, **49**, 265–280.
41. Bijsterbosch,M.K., Rump,E.T., De Vrueh,R.L., Dorland,R., van Veghel,R., Tivel,K.L., Biessen,E.A., van Berkel,T.J. and Manoharan,M. (2000) Modulation of plasma protein binding and in vivo liver cell uptake of phosphorothioate oligodeoxynucleotides by cholesterol conjugation. *Nucleic Acids Res.*, **28**, 2717–2725.
42. Yu,R.Z., Lemonidis,K.M., Graham,M.J., Matson,J.E., Crooke,R.M., Tribble,D.L., Wedel,M.K., Levin,A.A. and Geary,R.S. (2009) Cross-species comparison of in vivo PK/PD relationships for second-generation antisense oligonucleotides targeting apolipoprotein B-100. *Biochem. Pharmacol*, **77**, 910–919.
43. Shemesh,C.S., Yu,R.Z., Gaus,H.J., Seth,P.P., Swayze,E.E., Bennett,F.C., Geary,R.S., Henry,S.P. and Wang,Y. (2016) Pharmacokinetic and pharmacodynamic investigations of ION-353382, a model antisense oligonucleotide: Using Alpha-2-Macroglobulin and murinoglobulin Double-Knockout mice. *Nucleic Acid Ther.*, **26**, 223–235.
44. Donner,A.J., Wancewicz,E.V., Murray,H.M., Greenlee,S., Post,N., Bell,M., Lima,W.F., Swayze,E.E. and Seth,P.P. (2017) Co-Administration of an excipient oligonucleotide helps delineate pathways of productive and nonproductive uptake of phosphorothioate antisense oligonucleotides in the liver. *Nucleic Acid Ther.*, **27**, 209–220.